NASA Contractor Report 3518

Laminar Flow Transition: A Large-Eddy Simulation Approach

Sedat Biringen

CONTRACT NAS1-16289
FEBRUARY 1982

NASA

NASA Contractor Report 3518

Laminar Flow Transition: A Large-Eddy Simulation Approach

Sedat Biringen
Nielsen Engineering & Research, Inc.
Mountain View, California

Prepared for
Langley Research Center
under Contract NAS1-16289

National Aeronautics
and Space Administration

**Scientific and Technical
Information Branch**

1982

CONTENTS

SUMMARY 1

1. INTRODUCTION 2

2. SOLUTION PROCEDURE 4

3. RESULTS 8

3.1 Test Cases for the Plane Poiseuille Flow (No Suction-Blowing) 8

3.2 Test Case with Suction-Blowing 12

4. STUDY OF SUBGRID SCALE MODEL AND LENGTH SCALE 15

5. CONCLUSIONS 18

REFERENCES 19

TABLE 1 20

FIGURES 1 THROUGH 10 21

SUMMARY

A vectorized, semi-implicit code is developed for the solution of the time-dependent, three-dimensional equations of motion in plane Poiseuille flow by the large-eddy simulation technique. The code is tested by comparing results with those obtained from the solutions of the Orr-Sommerfeld equation. Comparisons indicate that finite-differences employed along the cross-stream direction act as an implicit filter. This removes the necessity of explicit filtering along this direction (where a nonhomogeneous mesh is used) for the simulation of laminar flow transition which includes nonlinear effects.

1. INTRODUCTION

This report is a summary of work on the computation of laminar flow control (LFC) by suction and laminar flow transition. We consider the time-dependent, three-dimensional equations of motion for incompressible, plane Poiseuille flow and solve these equations numerically by the large-eddy simulation technique. The main features of the solution procedure involve the use of the pseudo-spectral technique to evaluate spatial derivatives along homogeneous directions and finite differences along the nonhomogeneous direction, solving the continuity equation directly and transformation of the finite difference equations into wave-number space to reduce the partial differential equation set to a set of ordinary differential equations which are solved by block tridiagonal matrix inversion. It should be noted that although the present approach makes use of the large-eddy simulation technique which enables it to be valid for both laminar and turbulent flows, during this contract period we have performed calculations only for laminar flow stability for code testing. The incorporation of a subgrid scale turbulence model, which can be conveniently done by simply changing one subroutine, is necessary for turbulent flow computations.

It is generally accepted that transition of laminar flow to turbulent flow involves a number of intermediate stages. The initial stage is characterized by the existence of two-dimensional Tollmien-Schlichting waves which become weakly three-dimensional in the second stage. This is followed by the third stage in which the Tollmien-Schlichting waves become fully three-dimensional. In the fourth stage high shear-layers with

inflexional velocity profiles are developed and these shear-layers produce secondary instabilities in the fifth stage. Finally, the last stage is the breakdown of three-dimensional wave pattern into turbulence.

Mechanisms and phenomena that follow the amplification of the Tollmien-Schlichting waves and that finally lead to the fully developed turbulent flow cannot be predicted by linear theory. The theoretical understanding and prediction methods for this increasingly three-dimensional flow in which nonlinear effects play a dominant role do not show close agreement with experimental observations. Hence, although the behavior of small amplitude disturbances on laminar flow stability is well understood, there is as yet no close agreement between theoretical and experimental studies of the behavior of finite-amplitude disturbances and their effect on transition.

This work involves a complete simulation of laminar flow transition to turbulence, including nonlinear effects and as reported here involves the following tasks:

(1) Vectorization of the channel flow solution procedure of reference 3 for the CYBER-203 computer at NASA/Langley Research Center.

(2) Development and formulation of various initial conditions required for the calculation of the transition and LFC.

(3) Preliminary calculations for laminar flow stability for code testing purposes.

(4) Definition and implementation of required wall-boundary conditions for LFC by suction.

(5) An initial study of subgrid scale model and length scale.

All the calculations reported herein were performed on a 32x33x32 mesh. The objective of these calculations have been to test the code, e.g. with regard to speed and efficiency, as well as accuracy and stability for various boundary conditions. Calculations were performed with arbitrary periodic initial conditions that satisfy no-slip conditions and with initial conditions that are the eigensolutions of the Orr-Sommerfeld equation. These are reported in section 3, whereas section 2 contains a brief description of the solution procedure.

2. SOLUTION PROCEDURE

In large-eddy simulation of turbulent flows, each flow variable is decomposed into a large-scale component and a residual-field component. This can be obtained by filtering the flow variables, u_i and p (where u_i are the velocity components along x_i and p is the pressure) such that

$$u_i(\underset{\sim}{x},t) = \bar{u}_i + u'(x,t) \tag{1}$$

and

$$\bar{u}_i(x,t) = \int_D G(\underset{\sim}{x}-\underset{\sim}{x}')u_i(x',t)d\underset{\sim}{x}' \tag{2}$$

In these expressions u_i' is the residual-field component, $\bar{u}_i$ is the large-scale (filtered) component, and $G(\underset{\sim}{x},\underset{\sim}{x}')$ is the Gaussian filter function. If this filtering operation is applied to the incompressible Navier-Stokes equations one obtains

Momentum: $$\frac{\partial \bar{u}_i}{\partial t} + \overline{\bar{u}_j \frac{\partial \bar{u}_i}{\partial x_j}} = - \frac{\partial \tilde{p}}{\partial x_i} - \frac{\partial}{\partial x_j} \tau_{ij} + \frac{\partial^2 \bar{u}_i}{\partial x_j \partial x_j} \qquad (3)$$

Continuity: $$\frac{\partial \bar{u}_i}{\partial x_i} = 0 \qquad (4)$$

Here τ_{ij} is the subgrid scale (SGS) stress tensor, and density, ρ, is imbedded into the definition of $\tilde{p}$. The equations will be closed once τ_{ij} is modeled. In reference 3 for the large-eddy simulation of turbulent channel flow, an eddy viscosity type model is used for τ_{ij}. In this model, the eddy viscosity, ν_T, is directly written as a function of $\bar{S}_{ij}$, which is the strain rate tensor of the large-scale field. Owing to this strong coupling between the SGS-stresses and large-scale field, this model absorbs too much energy from the large-scale motion and inhibits evolution and development of turbulent flow. The prescription of an appropriate model which represents the correct dynamics of the flow field will be a major part of our second-year work.

The main task performed was the development of a vectorized computer code for efficient numerical integration of equations (3) and (4). These equations are written in a form which will conserve energy, e.g.

Momentum:

$$\frac{\partial u_i}{\partial t} = H_i - \frac{\partial p}{\partial x_i} + \left[(1+\delta_{i2})\tilde{\nu}_T + \frac{1}{Re}\right] \frac{\partial^2 u_i}{\partial x_2^2} + \frac{1}{Re}\left(\frac{\partial^2 u_i}{\partial x_1^2} + \frac{\partial^2 u_i}{\partial x_3^2}\right) \qquad (5)$$

Continuity:

$$\frac{\partial u_i}{\partial x_i} = 0 \qquad (6)$$

Here Re is the Reynolds number based on channel centerline velocity, U_o, channel half-width, δ, and kinematic viscosity, ν. H_i is a function that contains the convective terms, i.e., all the SGS terms along x_1 and x_3 and part of the SGS terms, i.e., all For convenience, we have dropped the overbar from the filtered variables. We have used a semi-implicit algorithm to numerically solve equations (5) and (6). This procedure employs the following finite difference formulae for time-advancement.

i) For H_i: Explicit Adams-Bashforth
ii) For $\partial p/\partial x_i$: Implicit Crank-Nicolson
iii) For $\partial^2 u_i/\partial x_1^2$, $\partial^2 u_i/\partial x_2^2$, $\partial^2 u_i/\partial x_3^2$: Implicit Crank-Nicolson
iv) $\tilde{\nu}_T$ is evaluated at the previous time-level

The solution procedure assumes the flow to be homogeneous along x_1- and x_3-directions and makes use of the pseudo-spectral technique to calculate space derivatives along these directions via fast Fourier transforms (FFT). Three-point central-difference operators are used along the x_2-direction. Figure 1 shows a schematic of the flow field geometry.

Once the governing equations are discretized in time, we employ a 2-D FFT along x_1 and x_3 and transform the equations into the wave-number space, k_1, k_3. This transformation enables one to obtain a set of ordinary differential equations along x_2 which is solved for every pair of k_1 and k_3.

Hence to solve both imaginary and real parts of the dependent variables, two sweeps through the data base are required. During these sweeps a block-tridiagonal system must be solved for each pair of k_1 and k_3 along the x_2-direction. A special solution technique is employed for $k_1 = k_3 = 0$, for which a scalar tridiagonal system is solved separately.

It should be noted that the solution procedure involves three main mathematical operations which had to be vectorized.

(1) One-dimensional Fast Fourier Transform: This is used to evaluate the derivatives along the x_1- and x_2-directions by the pseudo-spectral technique. For this purpose we have implemented the STAR library subroutine Q4FFORMS, which is recommended to be used for a large number of systems, each consisting of a large number of independent transforms.

(2) Two-dimensional Fast Fourier Transform: For the transformation of the difference form of equations (5) and (6), we have employed the STAR library subroutine Q4FFT2DR, which minimizes array storage by making use of the two-dimensional Fourier transform properties of a real field.

(3) Block-Tridiagonal matrix inversion along x_2: Note that the governing equations can be written in the following vector form,

$$\underline{A}\ \underset{\sim}{F}^{n+1}_{K+1} + \underline{B}\ \underset{\sim}{F}^{n+1}_{K} + \underline{C}\ \underset{\sim}{F}^{n+1}_{K-1} = R \qquad (7)$$

In equation (7) F is the solution vector whose components are u_1, u_2, p; R is the right-hand-side vector that contains the convective terms and part of the viscous terms. $\underline{A}$, $\underline{B}$, $\underline{C}$ are coefficient matrices whose components are functions of the kinematic viscosity, ν, and wave numbers k_1 and k_3. The solution procedure requires the inversion of this block-tridiagonal system along x_2 for each k_1 and k_3 in two passes, once for real parts of u_1,u_3 imaginary parts u_2,p and once for imaginary parts of u_1,u_3 real parts u_2,p. In the vectorization process we have used a vectorized subroutine developed by J. Lambiotte (in a private communication) which enables the inversion of a large number of tridiagonal systems simultaneously decreasing the number of scalar operations required to invert each system separately. This results in a very substantial reduction in CPU time. In implementing this subroutine we have found it to be most efficient to do the inversion at two x_1 - x_3 planes simultaneously only once for both passes. This was done by a DO-LOOP such that at each

index of the DO LOOP a total of 62 tridiagonal systems are inverted.

In addition to these, the rest of the program has been written in STAR-FORTRAN which makes extensive use of explicit vector statements to decrease CPU time. The current program requires about 5 seconds of CPU time and 3 CRU per time-step on the CYBER-203, including input-output.

3. RESULTS

3.1 Test Cases for the Plane Poiseuille Flow (No Suction-Blowing)

To test the computer code developed during the first year, we have performed a number of preliminary computations. The results of the cases without suction-blowing are contained in this section.

As the first test we have chosen the calculation of entry flow in a channel as a model problem and prescribed the following initial conditions at Re = 100

$$u_1 = C(1 - x_2^8) + \varepsilon L_1 \sin(\pi x_2) \cos\left(4\pi \frac{x_1}{L_1}\right) \sin\left(2\pi \frac{x_3}{L_3}\right) \quad (8)$$

$$u_2 = -\varepsilon(1 + \cos \pi x_2) \sin\left(4\pi \frac{x_1}{L_1}\right) \sin\left(2\pi \frac{x_3}{L_3}\right) \frac{L_1}{\pi} \quad (9)$$

$$u_3 = -\varepsilon L_3 \sin\left(4\pi \frac{x_1}{L_1}\right) \sin(\pi x_2) \cos\left(2\pi \frac{x_3}{L_3}\right) \quad (10)$$

where $L_1 = 2\pi$ and $L_3 = 4\pi/3$ are the box lengths along the homogeneous directions x_1 and x_3, respectively. The value of the constant, ε, was taken equal to about 5% of the maximum velocity in the channel.

Results of this case are presented in figures 2 and 3. Figure 2 shows the evolution of the mean velocity profile, $\langle u_1 \rangle$, and indicates that with increasing time-steps the parabolic velocity profile of the fully developed channel will be recovered. The time-history of the turbulent statistics (ref. 1) shows that the disturbance energy rapidly decays with time as expected.

During this code verification phase we have performed a second calculation by using the two-dimensional Orr-Sommerfeld solutions as the initial conditions. The complex frequency, ω, is an output of the solution procedure and represents the eigenmode of the flow for given α, β, Re and $U(x_2)$. For this calculation we have selected Re = 1500, $\alpha = 1$ and $\beta = 0$. The Orr-Sommerfeld code (ref. 2) gives the distribution of $\hat{u}_2$ and ω, $\omega = -0.32630 + 0.02821\ i$, as the solution for this case. Since $\tilde{u} = \hat{u}_i(y)e^{i\alpha(k-\omega t)}$, the imaginary part of ω determines the nature of the solution. For this case, $\hat{u}_i \sim e^{-0.0281}$, and the solution decays in time.

Using the initial conditions generated as explained above, we have performed a series of calculations using our code. Along the x_2-direction we have used a mesh clustering of the form

$$Y_J = \frac{1}{A} \tanh[\eta_J \tanh^{-1}(a)]$$

where Y_J is the x_2 coordinate in the physical plane and η_J is the x_2 coordinate in the stretched plane (uniform mesh spacing). In these calculations we have used A = 0.8, which gives $(\Delta x)_{min} \simeq 0.035$.

It should be noted that the time-advancement scheme we employ is partly explicit and partly implicit. Although in light of linear stability analysis, implicit methods are

sometimes advocated to be unconditionally stable, time-accuracy requires adherence to stability bounds of explicit schemes. In all the calculations reported here, we have obeyed both the convective stability requirement (the Courant-Friedrichs-Lewy conditions) and the diffusive stability requirement. At each time-step for the former we used

$$\text{C.N.} \equiv \Delta T \left[\left| \frac{u_1}{\Delta x_1} \right| + \left| \frac{u_2}{\Delta x_2} \right| + \left| \frac{u_3}{\Delta x_3} \right| \right]_{\max} \leq 0.35 \qquad (11)$$

where C.N. is the Courant number. For diffusive stability we used

$$D = \frac{1}{Re} \left[\frac{\Delta T}{\Delta x_2^2} \right]_{\max} \leq 0.1 \qquad (12)$$

With $(\Delta x_2)_{\min} \approx 0.035$ we have found it sufficient to use $0.02 \leq \Delta T \leq 0.04$ to satisfy both of the above stability criteria.

In choosing the periodicity length (the box length) we set the smallest wave number allowed in the computational domain equal to α (along x_1 and x_3). This corresponds to the longest wavelength allowed, i.e., the one whose wavelength is equal to the periodicity length.

Results for this case are summarized in figures 4 and 5. Figure 4 shows the plot of $u_1(x_2)$ at two instances in time; the solid curve corresponds to the initial disturbance at T = 0 and the broken line is at T = 260, which corresponds to a phase shift of π. The shape of the disturbance distribution is well preserved and a strong decay is also indicated. Accordingly the computed phase angle is equal to 0.291, as opposed to the exact solution, 0.3263 (which is the real part of ω).

In figure 5, time-history of plane averaged disturbance-velocity components are plotted. These show that the disturbance energy decays almost exponentially (as expected from the linear theory) except in the region $T < 2.5$. The computed results decay at a rate about twice as fast as the Orr-Sommerfeld solution shown as the solid line. The reasons for this will be explained later.

A series of calculations with finite-amplitude disturbances were also made for a test case which was run for identical input conditions as Run No. 2 of reference 3. These conditions are summarized in Table 1.

Results for this case are contained in figures 6 to 9. Figure 6 shows the time-history of average disturbance intensities, $\langle \hat{u}_1^2 \rangle$ and $\langle \hat{u}_3^2 \rangle$ and indicate a strong damping of these quantities. Figure 7 shows a comparison of the present calculations with those of reference 3 for the time-history of the maximum amplitude of $\hat{u}$. The computations of reference 3 indicate that after an initial transient period, the disturbance grows slowly. Our calculations, however, show a strong damping of the initial disturbance. This behavior of our computations is very similar to the previous case in which the decay rate of small amplitude disturbances was found to be much faster than indicated by the Orr-Sommerfeld solution.

Figure 8 shows the time-history $\langle \hat{u}_2^2 \rangle$ and indicates a fast growth for this quantity. This lends some support to the findings of reference 3, such that an initially two-dimensional finite amplitude disturbance may be driven to instability by three-dimensional effects caused by round-off errors. In this case, the most likely source of round-off errors are the Fourier transform operations.

Finally, in figure 9 a plot of profiles of $\langle \hat{u}_1 \rangle$ is presented at three instants in time. The shape of the initial

profile is well preserved, and a strong amplitude decay is displayed.

The test cases presented herein have indicated that our results are more dissipative than both the Orr-Sommerfeld solutions and the results of reference 3. It should, however, be noted that the method of reference 3 employs Chebyshev polynomials along the cross-stream direction so that the accuracy of spatial derivatives is "infinite order" with respect to the second-order finite-difference scheme that is employed in our method along the cross-stream direction. Hence, we believe that the dissipative nature of our code is caused by the filtering effects of the finite-difference scheme. In fact, in computations of the complete transition process in which the governing equations will be filtered, this dissipative property will provide an implicit "filter" along the cross-stream direction. The governing equations will be formally filtered along the homogeneous directions only. For the case in which stability of laminar flow in the linear range is of interest, a more accurate method along the cross-stream direction seems necessary. This can be obtained either by increasing mesh points along this direction or by employing polynomial expansions for the flow field variables.

3.2 Test Case with Suction-Blowing

In order to implement suction boundary conditions, it must be recalled that our solution procedure employs homogeneous boundary conditions in the streamwise x_1 and the spanwise x_3 directions. This, of course, requires that the incoming mass flow rate must be equal to the outgoing mass flow rate. Hence, the continuity equation averaged over $x_1 - x_3$ planes gives

$$\frac{\partial \langle u_2 \rangle}{\partial x_2} = 0 \tag{13}$$

from which

$$\langle u_2 \rangle = \text{const.} \tag{14}$$

Equation (14) states that continuity can be preserved only if the average velocity at one wall is equal in both magnitude and direction to the average velocity at the other wall. Therefore, with this formulation, the only mathematically plausible physical problem is to apply suction at one wall and blowing at the other wall with equal magnitude.

The velocity boundary conditions take the form $u_1 = 0$, $u_3 = 0$, and $u_2 = f(x_1,x_3)$ where $f(x_1,x_3)$ can be any periodic function. The pressure boundary condition at each wall is obtained from the u_2 momentum equation evaluated at the first interior point away from the wall. An exact solution for plane-Poiseuille flow with suction-blowing boundary conditions can be obtained by integrating the equations of motion for steady, incompressible flow in a two-dimensional channel. This gives,

$$\hat{u}_1 = -\frac{1}{\text{Re}\ \hat{V}_c}\left\{\frac{\left[2e^{\text{Re}\ \hat{V}_c(1+\hat{x}_2)} - e^{2\text{Re}\ \hat{V}_c} - 1\right]}{\left[e^{2\text{Re}V_c} - 1\right]} - \hat{x}_2\right\} \tag{15}$$

Here the caret refers to a nondimensional quantity, and Re is the Reynolds number based on channel half-width and channel centerline velocity.

It should be noted that equation (15) becomes interdeterminate for $\hat{V}_c = 0$ which simulates flow in a channel without suction-blowing. However,

$$\lim_{\hat{V}_c \to 0} u_1 = (1-x_2^2) \tag{16}$$

Hence as $\hat{V}_c \to 0$ expression (16) recovers the parabolic velocity profile of the plane Poiseuille flow.

The suction-blowing boundary conditions were tested by performing calculations at Re = 100, $\hat{V}_c = 0.05$, where $\hat{V}_c$ is the suction velocity nondimensionalized by channel centerline velocity. The following initial conditions were used.

$$\hat{u}_1 = C(1 - x^2)$$

$$\hat{u}_2 = \hat{u}_c = 0$$

Note that these conditions simulate a fully developed channel flow which is subjected to suction at one wall and blowing at the other wall with equal velocity, $\hat{V}_c$. Calculations were performed with T = 0.006 (as in section 2.2) and results are presented in figure 10 at T = 0.3 which corresponds to 50 time-steps. In this figure the exact solution is also presented, and a very good agreement between the two solutions is displayed. As expected, in both cases the average velocity distribution is skewed and the location of maximum velocity has moved towards the suction-wall. The velocity gradients (in both cases) are considerably large at the suction-wall than at the blowing wall.

4. STUDY OF SUBGRID SCALE MODEL AND LENGTH SCALE

During this contract period we have made a preliminary study of a subgrid scale (SGS) turbulence model to be implemented into the code for the full simulation of transition. It should be noted that the type of SGS models in which the eddy viscosity is written as a function of the strain-rate of the large-scale motion extracts too much energy and inhibits the flow development. Considering the strong coupling between the filtered and unfiltered fields due to this type of SGS model, the use of a SGS model which relaxes this direct coupling will likely improve the calculation of transition. Moreover, it is desirable that a SGS model should be able to "turn on" itself due to some evolving property of the flow field which is characteristic of turbulence. Such an evolving quantity can be represented conveniently in terms of the kinetic energy of small-scale motion.

In this section, we formulate a SGS model which is derived from the transport equation for the kinetic energy, E, of the small-scale motion. We consider the equation

$$\underbrace{\frac{\partial E}{\partial t} + \bar{u}_k \frac{\partial E}{\partial x_k}}_{\text{convection}} - \underbrace{\nu\left[\frac{\partial^2 E}{\partial x_k^2} - \overline{\left(\frac{\partial u_i}{\partial x_k}\right)^2} + \left(\frac{\partial \bar{u}_i}{\partial x_k}\right)^2\right]}_{\text{dissipation } (\varepsilon)} = \underbrace{\frac{1}{2}\tau_{ij}\left(\frac{\partial \bar{u}_i}{\partial x_j} + \frac{\partial \bar{u}_j}{\partial x_i}\right)}_{\text{production } (P)}$$

$$\underbrace{- \frac{\partial}{\partial x_k}\left[\frac{\overline{u_k u_i^2}}{2} - \frac{\bar{u}_k \overline{u_i^2}}{2} - \bar{u}_i \overline{u_k u_i} + \bar{u}_i^2 \bar{u}_k + \frac{\overline{u_k p}}{\rho} - \frac{\bar{u}_k \bar{p}}{\rho}\right]}_{\text{velocity and pressure diffusion}} \qquad (17)$$

The turbulent channel flow is an equilibrium flow in which the contribution of the transport terms to the energy balance is much less than the other terms. Also since the effect of the SGS terms is to provide a physically plausible "sink" term for energy lost from the large-scale motion, a detailed and time-accurate solution of the kinetic energy equation is likely not necessary. In this work, therefore, we intend to use the simplest form of equation (17) with temporal and transport terms neglected. This gives:

$$\text{Dissipation} = \text{Production}$$

With this simplification the only higher-order term to be modeled is the dissipation. To this end, we introduce the following relation

$$\varepsilon = C_D \frac{E^{3/2}}{L} [1 + C_3/Re] \tag{18}$$

where

$$Re \equiv \frac{E^{1/2} L}{\nu}$$

and C_D and C_3 are constants to be determined.

Note that formula (18) has the correct form near the wall, i.e., where $Re << 1$, and outside the wall region, i.e., where $Re >> 1$.

Another assumption is required to relate τ_{ij} (which is the quantity we need to calculate) to E (which is the quantity equation (17) calculates). For the constitutive relation between E and τ_{ij} we propose to employ a Prandtl-Kolmogorov

type formula such that

$$\tau_{ij} = -2\nu_T \bar{S}_{ij} \tag{19}$$

and the eddy viscosity ν_T is given as

$$\nu_T = C_2 L E^{1/2} \tag{20}$$

where C_2 is a constant to be determined from physical considerations. Finally a modification for the presence of the wall is needed to suppress the eddy viscosity very near the wall. This can be obtained by multiplying ν_T by a function f_ν, which can be defined as

$$f_\nu = [1 - \exp(-0.014\ \mathrm{Re})] \tag{21}$$

It should be noted that the use of the kinetic energy equation requires the definition of a length scale. To this end we intend to implement the following formula for L,

$$L = \left[\min(\Delta_1, \ell')\ \min(\Delta_3, \ell')\ \min(h_2, \ell')\right]^{1/3} \tag{22}$$

where ℓ' is Prandtl's mixing length (ref. 1),

$$\ell' = \begin{cases} 0.1 & y_w > 0.1/\kappa \\ \kappa y_w & y_w \leq 0.1/\kappa \end{cases} \tag{23}$$

In equation (22) Δ_1 and Δ_3 are filter widths in the x_1- and x_3-directions, h_2 is the grid size in the x_2-direction, y_w is the distance to the nearest wall and κ is the von Kármán constant equal to 0.4.

A final assessment of the model and final evaluation of model constants will be made.

5. CONCLUSIONS

A vectorized, semi-implicit code for simulating transition and laminar flow control by suction in plane Poiseuille flow is developed. The code takes about 5 sec. of CPU time and 3 CRU per time-step on the CYBER 203 for a grid of 32x33x32 mesh points.

The code has been tested with various boundary conditions (no-slip, suction-blowing) and initial conditions [(a) arbitrary periodic, (b) Orr-Sommerfeld eigensolutions] and has been found to be stable and fast-converging. Comparisons of the present results with the linear theory have shown that the present results are more dissipative than both the Orr-Sommerfeld solutions (the linear theory) and the results of reference 3. We attribute this to the "filtering effect" of finite-difference operators which are employed along the nonhomogeneous direction. For the full simulation process this "dissipative" property will provide an implicit filter along the cross-stream direction. The governing equations will be formally filtered along the homogeneous directions only. For the case in which stability of laminar flow in the linear rage is of interest, a more accurate method along the cross-stream direction seems necessary. This can be obtained either by increasing mesh points along this direction or by employing polynomial expansions for the flow field variables.

REFERENCES

1. Moin, P., Reynolds, W. C. and Ferziger, J. H.: Large Eddy Simulation of Incompressible Channel Flow. NASA CR-152190, 1978.

2. Reynolds, W. C.: Orrsom - A FORTRAN IV Program for Solution of the Orr-Sommerfeld Equation. Tech. Rept. No. FM-4 Dept. of Mechanical Engineering, Stanford University, Stanford, California, November 1969.

3. Orzsag, S. A. and Kells, L. A.: Transition to Turbulence in Plane Poiseuille and Plane Couette Flow. J. Fluid Mech., Vol. 96, 1980, p. 159.

Table 1.- Summary of Conditions for Test Case with Finite-Amplitude Disturbances

Reynolds number	2935
x_1-wave number ($\alpha \equiv 2\Pi/x$)	1.3231
x_3-wave number	0
Reω	0.4353
Imω	-0.01819
Initial amplitude (x_1-velocity)	.1175
Spatial resolution	32x33x32
Time step, ΔT	0.02
Final time, T	40

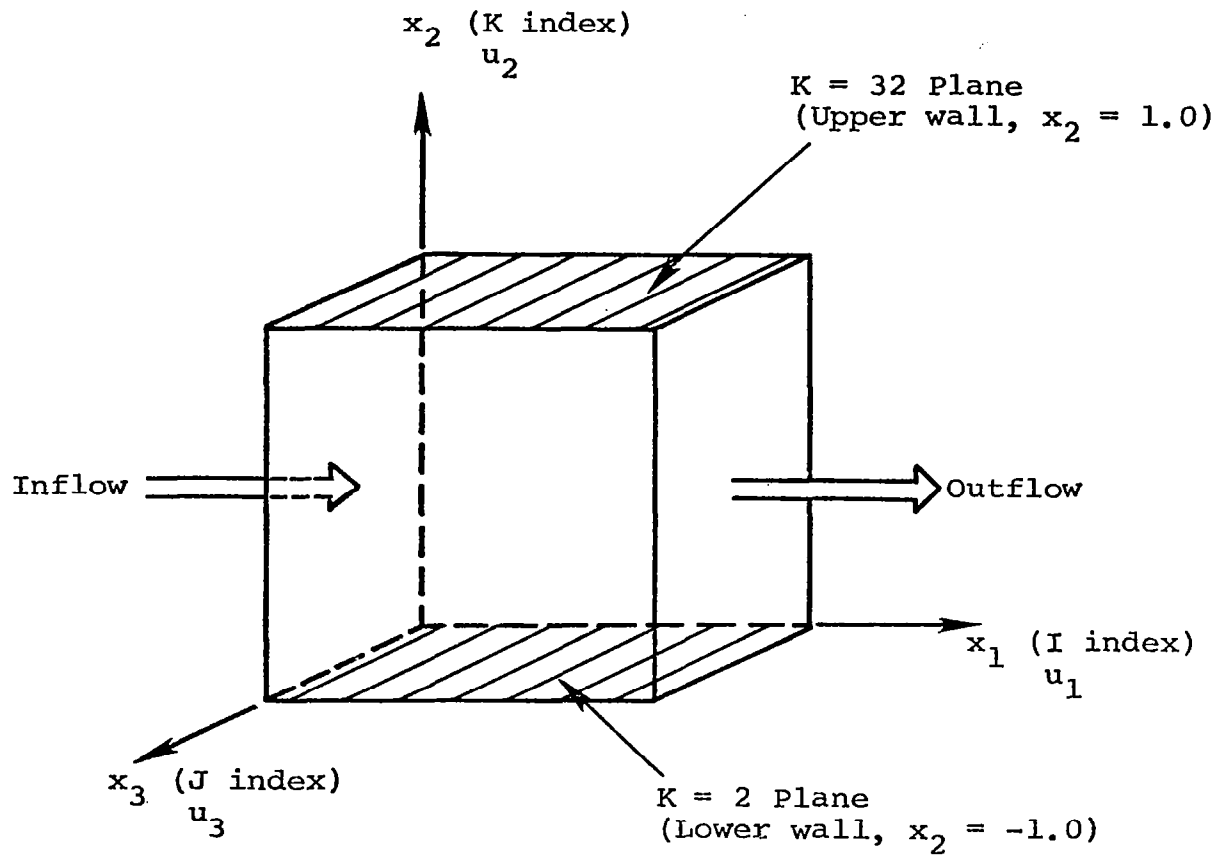

Figure 1.- Flow field geometry, the computational box.

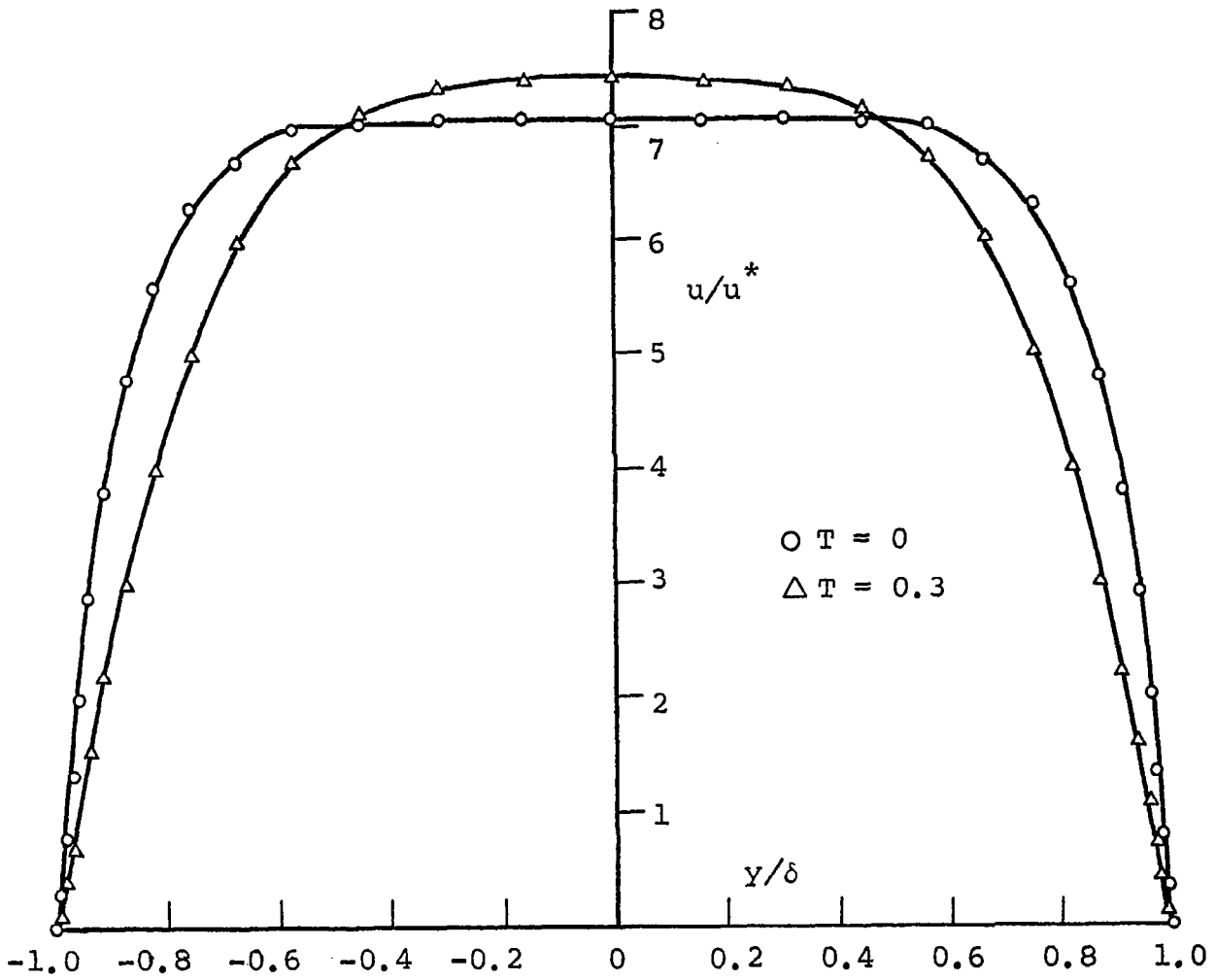

Figure 2.- Entry flow in a plane channel with 3-D disturbances.

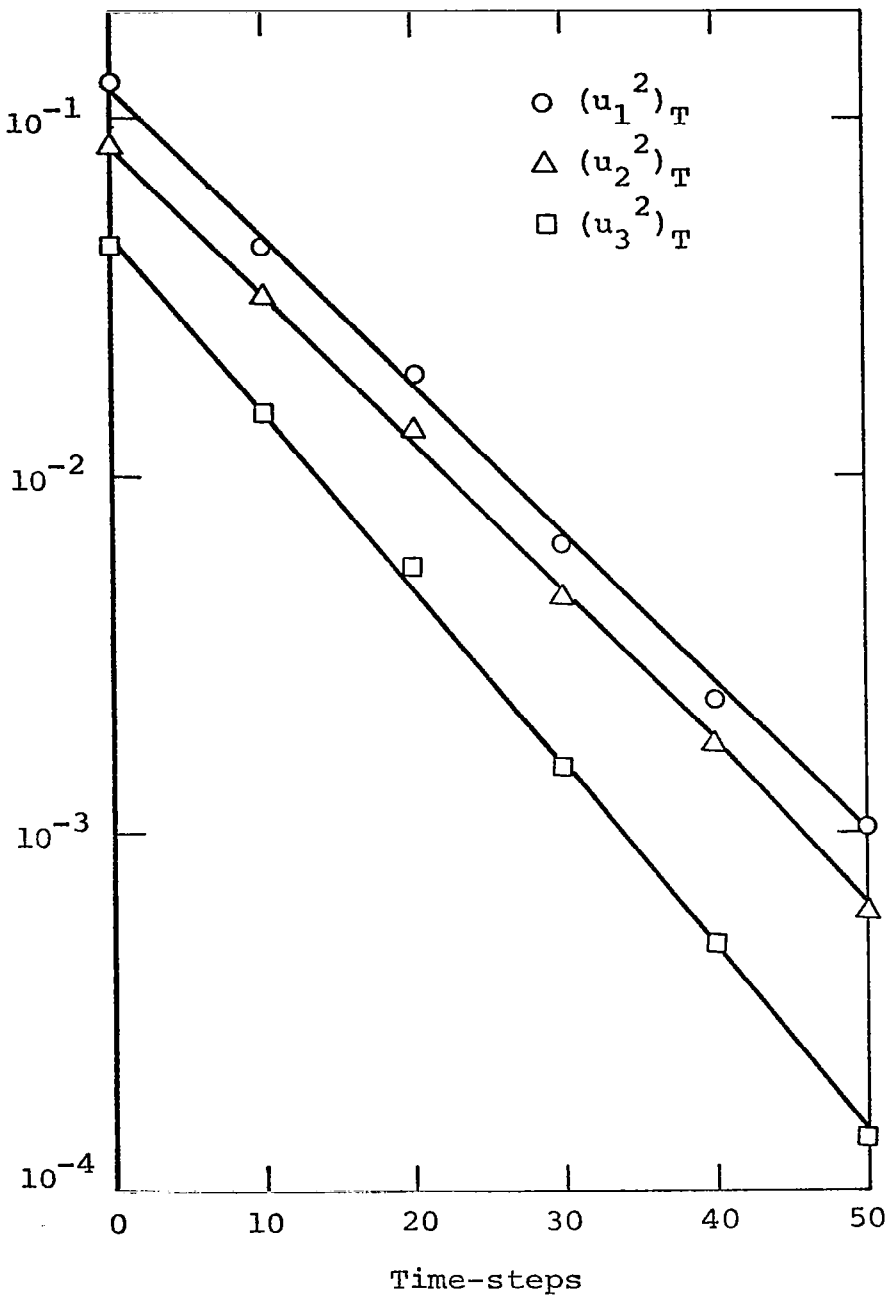

Figure 3.- Time-history of disturbance energy.

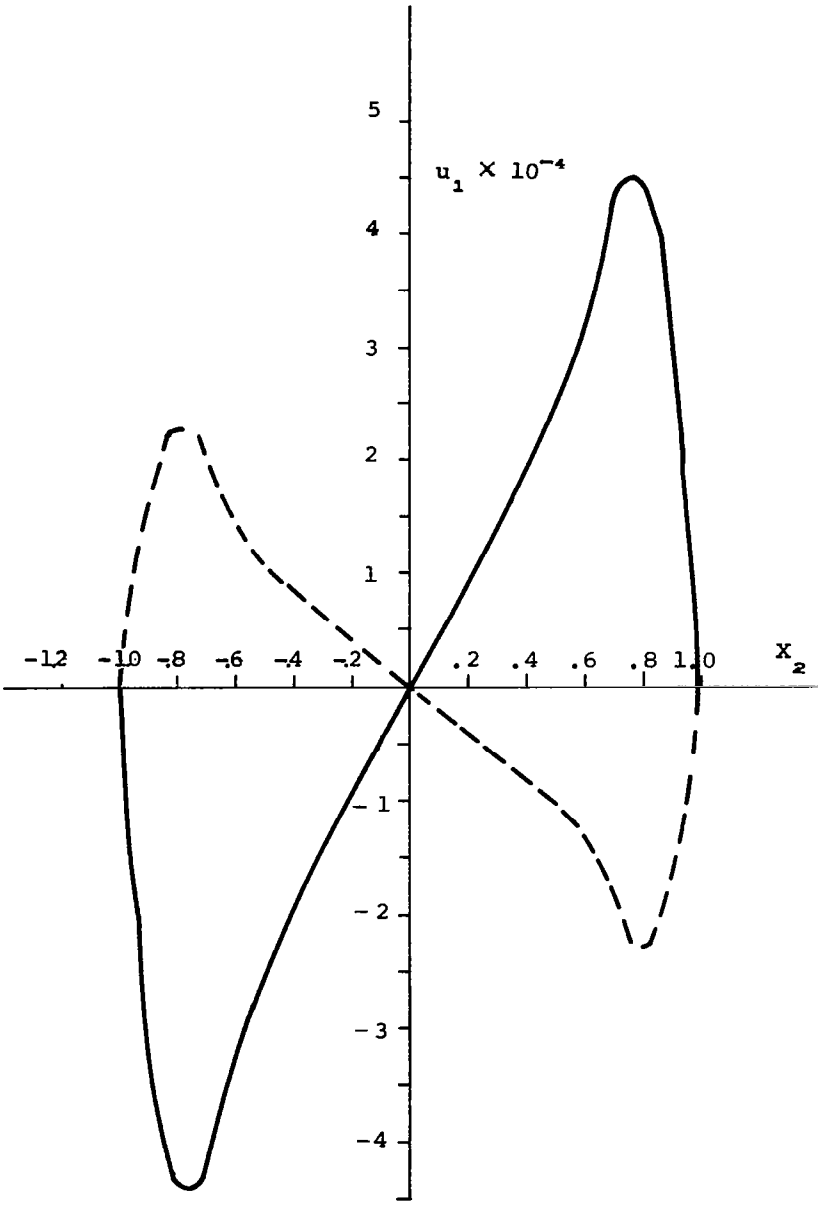

Figure 4.- A plot of the profile of $u_1(x_2)$, for the small disturbance case; ——, initial disturbance, — —, at $t = 10.8$, which corresponds to a computed phase angle of π.

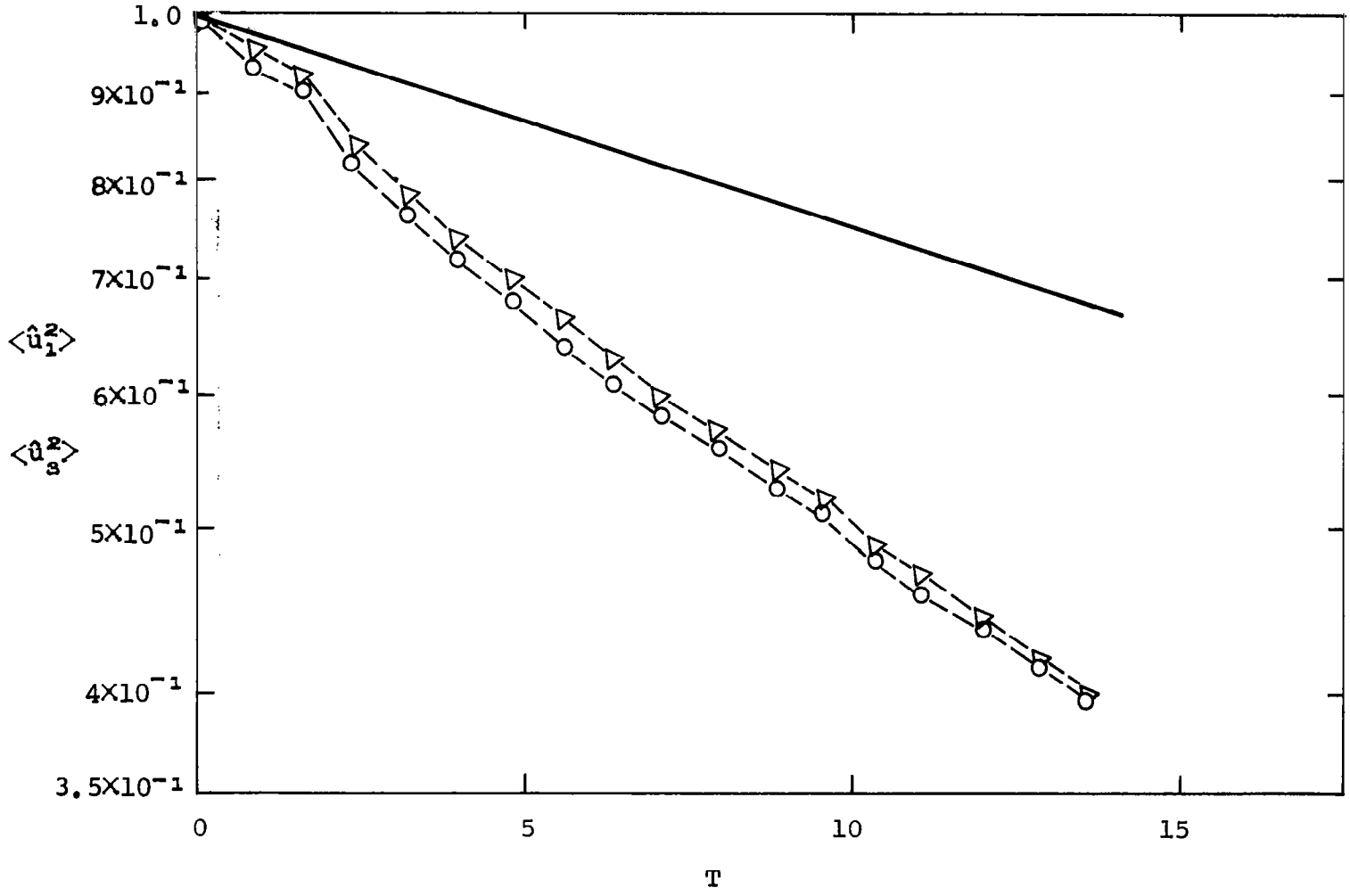

Figure 5.- Time-history of average disturbance intensities o-- , $\langle \hat{u}_1^2 \rangle$; Δ-- , $\langle \hat{u}_s^2 \rangle$; ——, Orr-Sommerfeld solution.

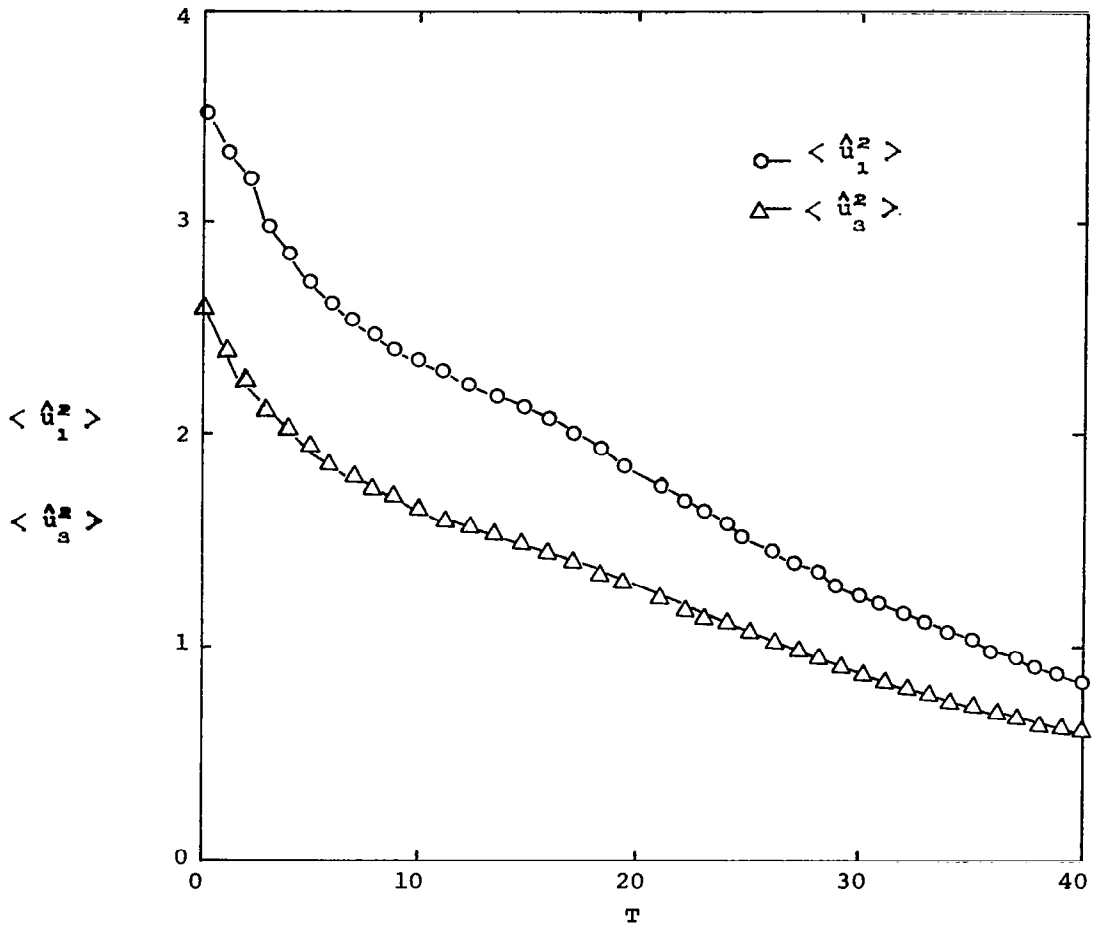

Figure 6.- Time-history of average disturbance intensities; finite amplitude case.

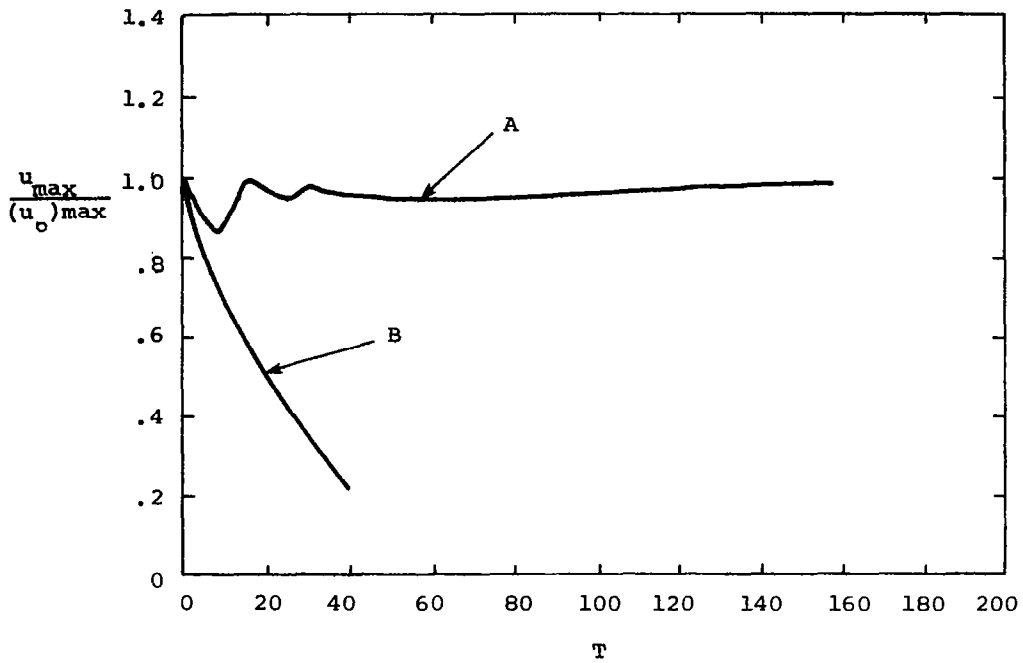

Figure 7.- Time-history of the maximum amplitude u_1 for finite amplitude disturbances: (A) computations of reference 3; (B) present results.

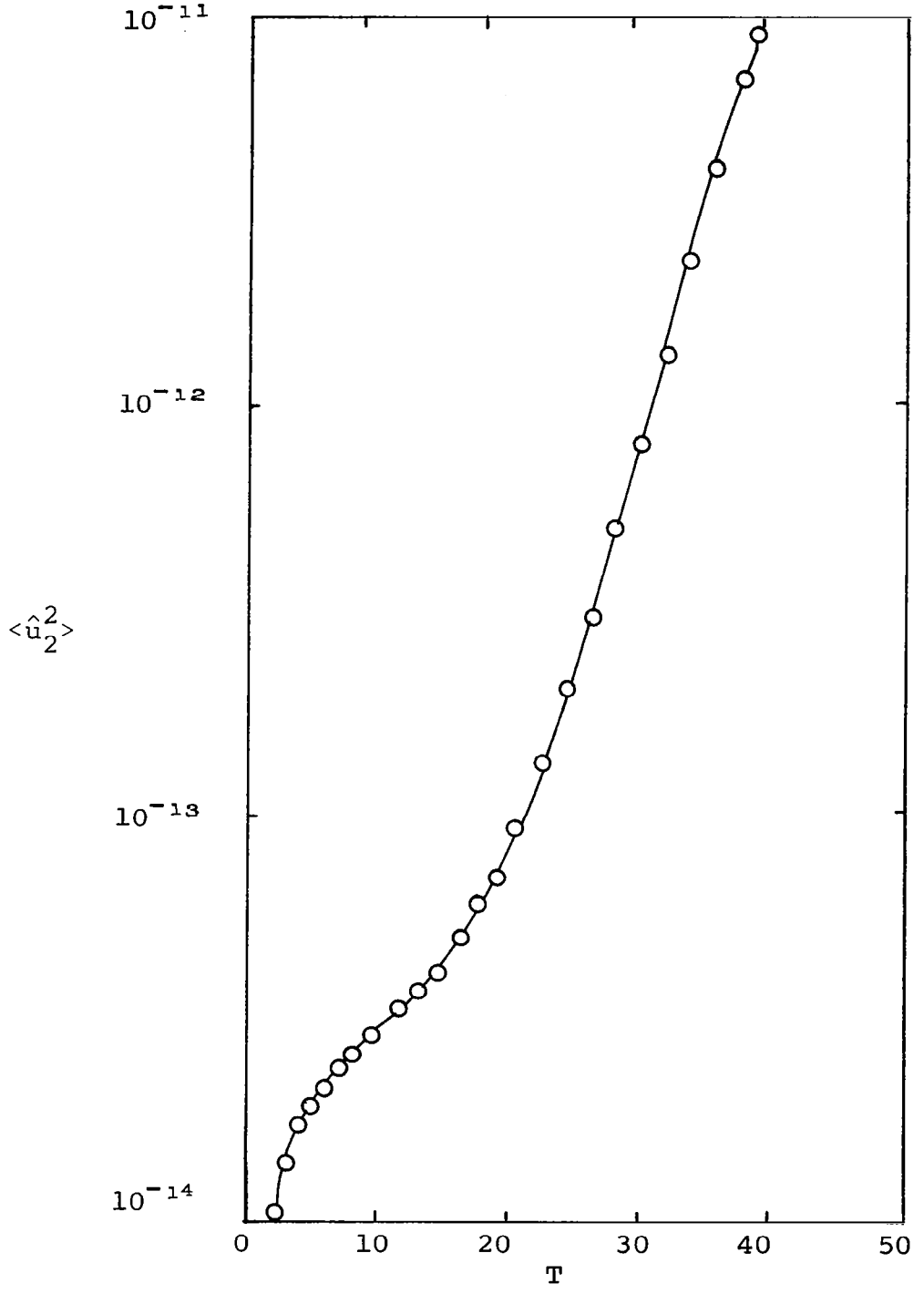

Figure 8.- Time history of $\langle \hat{u}_2^2 \rangle$.

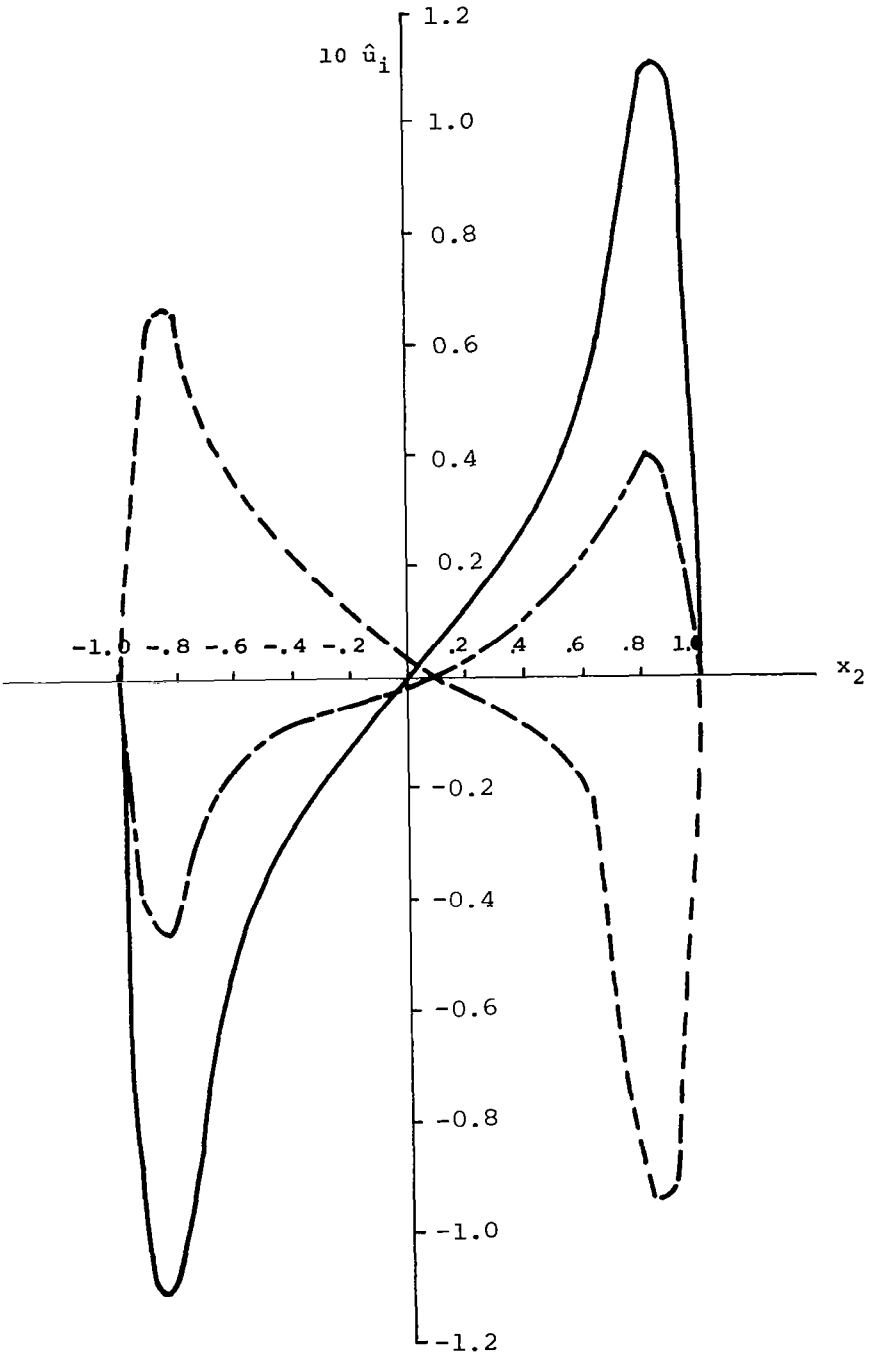

Figure 9.- A plot of the profile of $\hat{u}_1(x_2)$ for finite amplitude disturbance case; ——, initial disturbance; — —, at T = 8; — –, at 30.2.

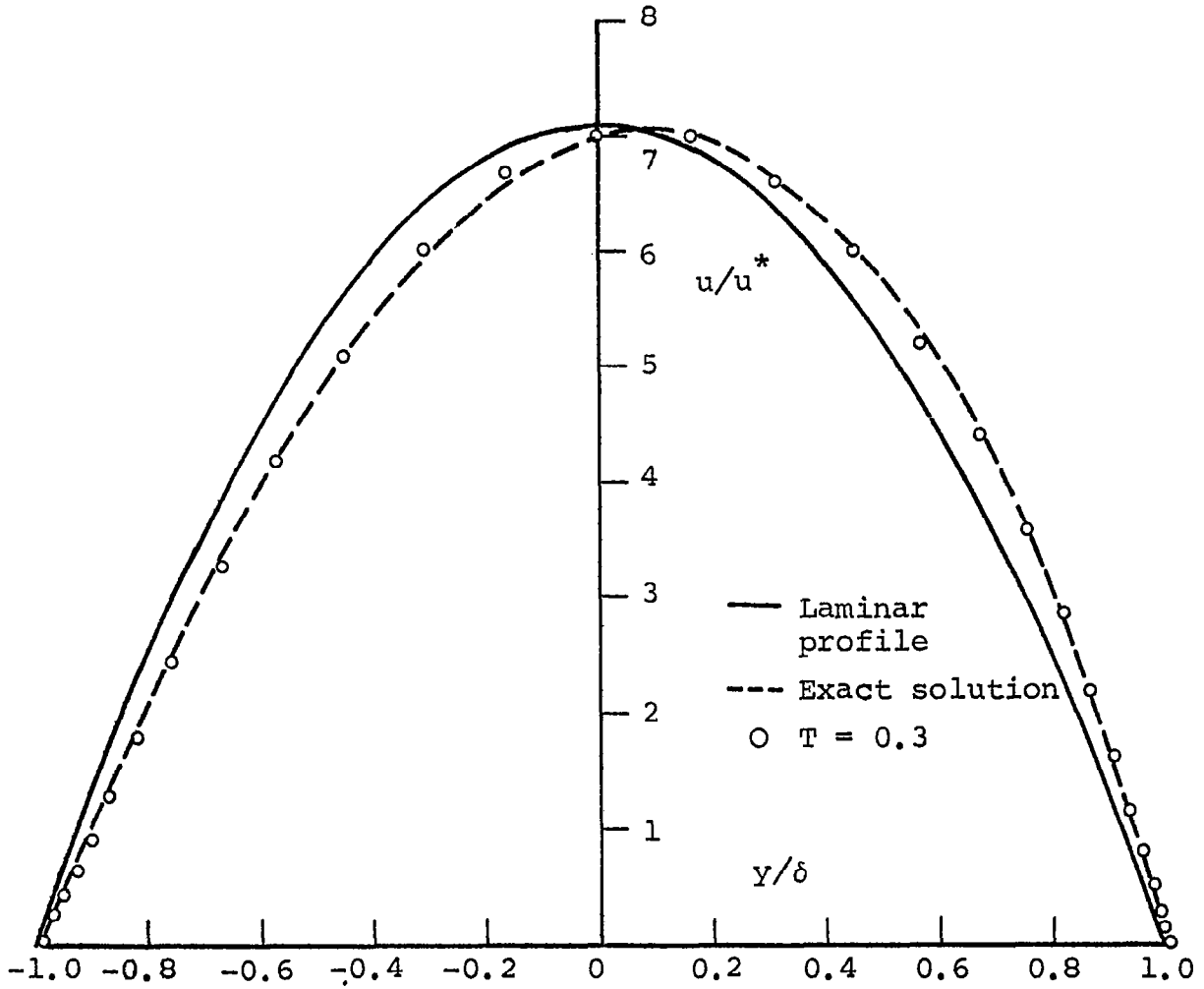

Figure 10.- Laminar flow in channel with suction, V_c/u_o = 0.01, Re = 100.

1. Report No.	2. Government Accession No.	3. Recipient's Catalog No.
NASA CR-3518		

4. Title and Subtitle	5. Report Date
LAMINAR FLOW TRANSITION: A LARGE-EDDY SIMULATION APPROACH	February 1982
	6. Performing Organization Code 652/C
7. Author(s)	8. Performing Organization Report No.
Sedat Biringen	NEAR TR 251
	10. Work Unit No.
9. Performing Organization Name and Address	11. Contract or Grant No.
Nielsen Engineering & Research, Inc. 510 Clyde Avenue Mountain View, California 94043	NAS1-16289
	13. Type of Report and Period Covered
12. Sponsoring Agency Name and Address	Contractor Report 7/14/1980 - 9/30/1981
National Aeronautics and Space Administration Washington, DC 20546	14. Sponsoring Agency Code

15. Supplementary Notes

Langley Technical Monitor: William D. Harvey
Final Report

16. Abstract

A vectorized, semi-implicit code is developed for the solution of the time-dependent, three-dimensional equations of motion in plane Poiseuille flow by the large-eddy simulation technique. The code is tested by comparing results with those obtained from the solutions of the Orr-Sommerfeld equation. Comparisons indicate that finite-differences employed along the cross-stream direction act as an implicit filter. This removes the necessity of explicit filtering along this direction (where a nonhomogeneous mesh is used) for the simulation of laminar flow transition into turbulence in which small scale turbulence will be accounted for by a subgrid scale turbulence model.

17. Key Words (Suggested by Author(s))	18. Distribution Statement
Calculation method Laminar flow transition Plane Poiseuille flow	Unclassified - Unlimited Subject Category 34

19. Security Classif. (of this report)	20. Security Classif. (of this page)	21. No. of Pages	22. Price
Unclassified	Unclassified	33	A03

For sale by the National Technical Information Service, Springfield, Virginia 22161

NASA-Langley, 1982